

University of Montana

## ScholarWorks at University of Montana

---

Forest Management Faculty Publications

Forest Management

---

4-22-2014

### Local spatial structure of forest biomass and its consequences for remote sensing of carbon stocks

M. Rejou-Mechain

*Universite Paul Sabatier (Toulouse III)*

H. C. Muller-Landau

*Smithsonian Tropical Resource Institute*

M. Dettlo

*Smithsonian Tropical Resource Institute*

Follow this and additional works at: [https://scholarworks.umt.edu/forest\\_pubs](https://scholarworks.umt.edu/forest_pubs)

 *Part of the Forest Management Commons*

**Let us know how access to this document benefits you.**

*Universite Paul Sabatier (Toulouse III)*

---

**Recommended Citation:**  
See next page for additional authors

Rejou-Mechain, M.; Muller-Landau, H. C.; Dettlo, M.; Thomas, S. C.; Toan, T. Le; Saatchi, S. S.; Barreto-Silvia, J. S.; Bourg, N. A.; Bunyavejchewin, S.; Butt, N.; Brockelman, W. Y.; Cao, M.; Cardenas, D.; Chiang, J.-M.; Chuyong, G. B.; Clay, K.; Condit, R.; Dattaraja, H. S.; Davies, S. J.; Duque, A.; Esufali, S.; Ewango, C.; Fernando, R.H.S.; Fletcher, C. D.; Gunatilleke, I.A.U.N.; Hao, Z.; Harms, K. E.; Hart, T. B.; Herault, B.; Howe, R. W.; Hubbell, S. P.; Johnson, D. J.; Kenfack, D.; Larson, A. J.; Lin, L.; Lin, Y.; Lutz, J. A.; Makana, J.-R.; Malhi, Y.; Marthews, T. R.; McEwan, R. W.; McMahon, S. M.; McShea, W. J.; Muscarella, R.; Nathalang, A.; Noor, N.S.M.; Nyctch, C. J.; Oliveira, A. A.; Phillips, R. P.; Pongpattananurak, N.; Punchi-Manage, R.; Salim, R.; Schurman, J.; Sukumar, R.; Suresh, H. S.; Suwanvecho, U.; Thomas, D. W.; Thompson, J.; Uriarte, M.; Valencia, R.; Vicentini, A.; Wolf, A. T.; Yap, S.; Yuan, Z.; Zartman, C. E.; Zimmerman, J. K.; and Chave, J., "Local spatial structure of forest biomass and its consequences for remote sensing of carbon stocks" (2014). *Forest Management Faculty Publications*. 47.

[https://scholarworks.umt.edu/forest\\_pubs/47](https://scholarworks.umt.edu/forest_pubs/47)

This Article is brought to you for free and open access by the Forest Management at ScholarWorks at University of Montana. It has been accepted for inclusion in Forest Management Faculty Publications by an authorized administrator of ScholarWorks at University of Montana. For more information, please contact [scholarworks@mso.umt.edu](mailto:scholarworks@mso.umt.edu).

---

## Authors

M. Rejou-Mechain, H. C. Muller-Landau, M. Detto, S. C. Thomas, T. Le Toan, S. S. Saatchi, J. S. Barreto-Silvia, N. A. Bourg, S. Bunyavejchewin, N. Butt, W. Y. Brockelman, M. Cao, D. Cardenas, J.-M. Chiang, G. B. Chuyong, K. Clay, R. Condit, H. S. Dattaraja, S. J. Davies, A. Duque, S. Esufali, C. Ewango, R.H.S. Fernando, C. D. Fletcher, I.A.U.N. Gunatilleke, Z. Hao, K. E. Harms, T. B. Hart, B. Herault, R. W. Howe, S. P. Hubbell, D. J. Johnson, D. Kenfack, A. J. Larson, L. Lin, Y. Lin, J. A. Lutz, J.-R. Makana, Y. Malhi, T. R. Marthews, R. W. McEwan, S. M. McMahon, W. J. McShea, R. Muscarella, A. Nathalang, N.S.M. Noor, C. J. Nyctch, A. A. Oliveira, R. P. Phillips, N. Pongpattananurak, R. Punchi-Manage, R. Salim, J. Schurman, R. Sukumar, H. S. Suresh, U. Suwanvecho, D. W. Thomas, J. Thompson, M. Uriarte, R. Valencia, A. Vicentini, A. T. Wolf, S. Yap, Z. Yuan, C. E. Zartman, J. K. Zimmerman, and J. Chave

This discussion paper is/has been under review for the journal Biogeosciences (BG).  
Please refer to the corresponding final paper in BG if available.

# Local spatial structure of forest biomass and its consequences for remote sensing of carbon stocks

M. Réjou-Méchain<sup>1</sup>, H. C. Muller-Landau<sup>2</sup>, M. Dett<sup>2</sup>, S. C. Thomas<sup>3</sup>, T. Le Toan<sup>4</sup>, S. S. Saatchi<sup>5</sup>, J. S. Barreto-Silva<sup>6</sup>, N. A. Bourg<sup>7</sup>, S. Bunyavejchewin<sup>8</sup>, N. Butt<sup>9,10</sup>, W. Y. Brockelman<sup>11</sup>, M. Cao<sup>12</sup>, D. Cárdenas<sup>13</sup>, J.-M. Chiang<sup>14</sup>, G. B. Chuyong<sup>15</sup>, K. Clay<sup>16</sup>, R. Condit<sup>2</sup>, H. S. Dattaraja<sup>17</sup>, S. J. Davies<sup>18</sup>, A. Duque<sup>19</sup>, S. Esufali<sup>20</sup>, C. Ewango<sup>21</sup>, R. H. S. Fernando<sup>22</sup>, C. D. Fletcher<sup>23</sup>, I. A. U. N. Gunatilleke<sup>20</sup>, Z. Hao<sup>24</sup>, K. E. Harms<sup>25</sup>, T. B. Hart<sup>26</sup>, B. Hérault<sup>27</sup>, R. W. Howe<sup>28</sup>, S. P. Hubbell<sup>2,29</sup>, D. J. Johnson<sup>16</sup>, D. Kenfack<sup>30</sup>, A. J. Larson<sup>31</sup>, L. Lin<sup>12</sup>, Y. Lin<sup>14</sup>, J. A. Lutz<sup>32</sup>, J.-R. Makana<sup>33</sup>, Y. Malhi<sup>9</sup>, T. R. Marthews<sup>9</sup>, R. W. McEwan<sup>34</sup>, S. M. McMahon<sup>35</sup>, W. J. McShea<sup>7</sup>, R. Muscarella<sup>36</sup>, A. Nathalang<sup>11</sup>, N. S. M. Noor<sup>23</sup>, C. J. Nytsch<sup>37</sup>, A. A. Oliveira<sup>38</sup>, R. P. Phillips<sup>16</sup>, N. Pongpattananurak<sup>39</sup>, R. Punchi-Manage<sup>40</sup>, R. Salim<sup>23</sup>, J. Schurman<sup>3</sup>, R. Sukumar<sup>17</sup>, H. S. Suresh<sup>17</sup>, U. Suwanvecho<sup>11</sup>, D. W. Thomas<sup>41</sup>, J. Thompson<sup>36,42</sup>, M. Uríarte<sup>36</sup>, R. Valencia<sup>43</sup>, A. Vicentini<sup>44</sup>, A. T. Wolf<sup>28</sup>, S. Yap<sup>45</sup>, Z. Yuan<sup>24</sup>, C. E. Zartman<sup>44</sup>, J. K. Zimmerman<sup>37</sup>, and J. Chave<sup>1</sup>

BGD  
11, 5711–5742, 2014

## Spatial sampling of forest biomass

M. Réjou-Méchain et al.

[Title Page](#)

[Abstract](#)

[Introduction](#)

[Conclusions](#)

[References](#)

[Tables](#)

[Figures](#)

[◀](#)

[▶](#)

[◀](#)

[▶](#)

[Back](#)

[Close](#)

[Full Screen / Esc](#)

[Printer-friendly Version](#)

[Interactive Discussion](#)



**Spatial sampling of forest biomass**

M. Réjou-Méchain et al.

[Title Page](#)[Abstract](#)[Introduction](#)[Conclusions](#)[References](#)[Tables](#)[Figures](#)[|◀](#)[▶|](#)[◀](#)[▶](#)[Back](#)[Close](#)[Full Screen / Esc](#)[Printer-friendly Version](#)[Interactive Discussion](#)

**Spatial sampling of forest biomass**

M. Réjou-Méchain et al.

[Title Page](#)[Abstract](#)[Introduction](#)[Conclusions](#)[References](#)[Tables](#)[Figures](#)[◀](#)[▶](#)[◀](#)[▶](#)[Back](#)[Close](#)[Full Screen / Esc](#)[Printer-friendly Version](#)[Interactive Discussion](#)

- <sup>19</sup>Departamento de Ciencias Forestales, Universidad Nacional de Colombia, Sede Medellín, Calle 59A No 63-20, Medellín, Colombia
- <sup>20</sup>Department of Botany, Faculty of Science, University of Peradeniya, Peradeniya, Sri Lanka
- <sup>21</sup>Centre de Formation et de Recherche en Conservation Forestière (CEFRECOF), Wildlife Conservation Society, Kinshasa, DR Congo
- <sup>22</sup>Royal Botanical Garden, Peradeniya, Sri Lanka
- <sup>23</sup>Forest Research Institute Malaysia (FRIM), 52109 Kepong, Selangor, Malaysia
- <sup>24</sup>State Key Laboratory of Forest and Soil Ecology, Institute of Applied Ecology, Chinese Academy of Sciences, Shenyang 110164, China
- <sup>25</sup>Department of Biological Sciences, Louisiana State University, Baton Rouge, LA 70803, USA
- <sup>26</sup>Project TL2, Kinshasa, DR Congo
- <sup>27</sup>Cirad, UMR Ecologie des Forêts de Guyane (EcoFoG), Campus Agronomique, BP701, 97310 Kourou, French Guiana
- <sup>28</sup>Department of Natural and Applied Sciences, University of Wisconsin-Green Bay, Green Bay, WI 54311, USA
- <sup>29</sup>Department of Ecology and Evolutionary Biology, University of California, Los Angeles, CA 90095, USA
- <sup>30</sup>CTFS-Arnold Arboretum Office, Harvard University, 22 Divinity Avenue, Cambridge, MA 02138, USA
- <sup>31</sup>Department of Forest Management, College of Forestry and Conservation, The University of Montana, Missoula, MT 59812, USA
- <sup>32</sup>Wildland Resources Department, Utah State University, 5230 Old Main Hill, Logan, UT 84322-5230, USA
- <sup>33</sup>Wildlife Conservation Society – DRC Program, Kinshasa, DR Congo
- <sup>34</sup>Department of Biology, University of Dayton, Dayton, OH 45469-2320, USA
- <sup>35</sup>Smithsonian Tropical Research Institute & Smithsonian Environmental Research Center, Edgewater, Maryland, USA
- <sup>36</sup>Department of Ecology, Evolution & Environmental Biology, Columbia University, New York, NY, USA
- <sup>37</sup>Department of Environmental Science, University of Puerto Rico, Box 70377, Rio Piedras, San Juan, 00936-8377, Puerto Rico

**Spatial sampling of forest biomass**

M. Réjou-Méchain et al.

[Title Page](#)[Abstract](#)[Introduction](#)[Conclusions](#)[References](#)[Tables](#)[Figures](#)[|◀](#)[▶|](#)[◀](#)[▶](#)[Back](#)[Close](#)[Full Screen / Esc](#)[Printer-friendly Version](#)[Interactive Discussion](#)

## Abstract

Advances in forest carbon mapping have the potential to greatly reduce uncertainties in the global carbon budget and to facilitate effective emissions mitigation strategies such as REDD+. Though broad scale mapping is based primarily on remote sensing data,

- 5 the accuracy of resulting forest carbon stock estimates depends critically on the quality of field measurements and calibration procedures. The mismatch in spatial scales between field inventory plots and larger pixels of current and planned remote sensing products for forest biomass mapping is of particular concern, as it has the potential to introduce errors, especially if forest biomass shows strong local spatial variation. Here,  
10 we used 30 large (8–50 ha) globally distributed permanent forest plots to quantify the spatial variability in aboveground biomass (AGB) at spatial grains ranging from 5 to 250 m (0.025–6.25 ha), and we evaluate the implications of this variability for calibrating remote sensing products using simulated remote sensing footprints. We found that  
15 the spatial sampling error in AGB is large for standard plot sizes, averaging 46.3 % for 0.1 ha subplots and 16.6 % for 1 ha subplots. Topographically heterogeneous sites showed positive spatial autocorrelation in AGB at scales of 100 m and above; at smaller scales, most study sites showed negative or nonexistent spatial autocorrelation in AGB.  
20 We further show that when field calibration plots are smaller than the remote sensing pixels, the high local spatial variability in AGB leads to a substantial “dilution” bias in calibration parameters, a bias that cannot be removed with current statistical methods. Overall, our results suggest that topography should be explicitly accounted for in future sampling strategies and that much care must be taken in designing calibration schemes if remote sensing of forest carbon is to achieve its promise.

## Spatial sampling of forest biomass

M. Réjou-Méchain et al.

[Title Page](#)

[Abstract](#)

[Introduction](#)

[Conclusions](#)

[References](#)

[Tables](#)

[Figures](#)

◀

▶

◀

▶

[Back](#)

[Close](#)

[Full Screen / Esc](#)

[Printer-friendly Version](#)

[Interactive Discussion](#)



# 1 Introduction

Forests represent the largest aboveground carbon stock in the terrestrial biosphere, and forest degradation and regrowth are globally important carbon fluxes (Pan et al., 2011). However, our ability to predict future atmospheric CO<sub>2</sub> concentrations or to implement effective carbon emission mitigation strategies (e.g. REDD+; Miles and Kapos, 2008) is limited by the accuracy of forest carbon stock estimates. The global monitoring of forest carbon stocks has thus come to the fore of the research agenda, with important implications in economics, policy and conservation (Gibbs et al., 2007). In recent years, aboveground carbon stock estimates based on field inventories and on remote sensing approaches have led to substantial progress in mapping broad-scale carbon stocks (Asner et al., 2010; Baccini et al., 2012; Malhi et al., 2006; Saatchi et al., 2011). However, substantial uncertainties are still associated with such carbon maps (Mitchard et al., 2013b).

Given the prohibitive cost of field and/or airborne campaigns to survey vegetation at broad spatial scales, space-based sensing of vegetation will probably soon dominate efforts to map and monitor forest carbon stocks beyond the landscape scale (Goetz and Dubayah, 2011; Wulder et al., 2012). Active remote sensing tools such as Light Detection and Ranging (LiDAR) and/or synthetic aperture radar (SAR) are currently the best candidates for forest carbon mapping at broad spatial scales. Two forthcoming spaceborne missions are thus of particularly interest: the LiDAR-based ICESAT2 mission (scheduled for launch in late 2015; Abdalati et al., 2010) and the P-band radar BIOMASS mission (scheduled for launch in 2020; Le Toan et al., 2011). Both instruments will have a relatively coarse resolution (50 m for ICESAT2 and 100–200 m for BIOMASS) and will rely on field data to calibrate their inversion models. Hence, the quality of the resulting forest carbon map will depend crucially on the accuracy and suitability of the field data used for calibration.

The quality of a field-based calibration and resulting products depends fundamentally on the degree to which forest biomass in entire pixels is represented by the field

## Spatial sampling of forest biomass

M. Réjou-Méchain et al.

[Title Page](#)

[Abstract](#)

[Introduction](#)

[Conclusions](#)

[References](#)

[Tables](#)

[Figures](#)

◀

▶

◀

▶

[Back](#)

[Close](#)

[Full Screen / Esc](#)

[Printer-friendly Version](#)

[Interactive Discussion](#)



data. In space-based remote sensing of forest biomass, sensor footprints are usually several to many times larger than field calibration plots (Baccini et al., 2007). If forest biomass is homogenous within pixel-sized areas, this mismatch in sample area will have little impact on calibration; however, if there is substantial local heterogeneity in biomass, then small ground samples will have large sampling errors. In general, the uncertainty associated with any field biomass estimate decreases as the sampling area increases. If sampling uncertainty is large, it is likely that the biomass maps calibrated using such field-based data will be unreliable. Furthermore, the remote sensing field of view is often different from the field-based one for several reasons including geolocalisation errors, the post-geoprocessing conversion of the ellipsoidal footprint into a square pixel, and the difference between the forest components measured (e.g. remote sensing canopy structure vs. field-based tree stem measurements; Mascaro et al., 2011). Such spatial mismatches may considerably increase the errors during the calibration step. There is thus a need to quantify these errors and test potential strategies to address them.

From a global perspective, ground sampling of forests is unevenly distributed. Over a million of forest inventory plots have been established across the temperate zone, with a high diversity in plot designs. For example, hundreds of thousands of permanent plots of approximately 0.1 ha are being monitored throughout the USA and Sweden (Bechtold and Patterson, 2005; Ranneby et al., 1987). However, in spite of the United Nations Food and Agricultural Organization Forestry programs, many areas, especially in the tropics, lack forest inventories. Individual scientists, sometimes working in collaborative networks, have collected data in hundreds of large plots ( $\geq 1$  ha) in the tropics (Condit, 1995; Lewis et al., 2009; Phillips et al., 2009). Though these collections of field plots do not represent systematic or random samples, they are routinely used to estimate forest carbon storage or to calibrate remote sensing models (Asner et al., 2013; Baccini et al., 2012; Chave et al., 2008; Malhi et al., 2006; Saatchi et al., 2011). Yet, little attention has been given to quantifying the error associated with the field sampling strategies, or to propagating this error to remote sensing estimates of carbon stocks

Spatial sampling of forest biomass

M. Réjou-Méchain et al.

[Title Page](#)

[Abstract](#)

[Introduction](#)

[Conclusions](#)

[References](#)

[Tables](#)

[Figures](#)

[◀](#)

[▶](#)

[◀](#)

[▶](#)

[Back](#)

[Close](#)

[Full Screen / Esc](#)

[Printer-friendly Version](#)

[Interactive Discussion](#)



(but for notable exceptions see Gonzalez et al., 2010; Mermoz et al., 2014). This is the focus of the present study.

Here, we applied spatial statistic methods to forest stand level census data from a global network of 30 large permanent plots (8 to 50 ha) established in natural forests (Condit, 1998; Losos and Leigh, 2004) to simulate the range of ground forest sampling strategies and explore related uncertainties (Fig. 1; Supplement, Table S1). Using these very large plots, we address three main questions: (1) how large are field-sampling errors in aboveground biomass (AGB) stock, how do they vary across sites, forest types, and continents, and how do they scale with the area sampled? (2) What is the local spatial structure of AGB, and how does this spatial structure vary among sites? (3) What are the implications of field sampling error for the accuracy of remote sensing calibration equations under different calibration plot and remote sensing footprint areas, and different bias-correction procedures?

## 2 Material and methods

### 2.1 Field data

We used standardized measurements in 30 large forest plots across three continents

(8–50 ha each, Fig. 1 and Table S1). In 28 of the plots, all free-standing trees  $\geq 1$  cm dbh (diameter measured to the nearest millimeter at 130 cm above the ground or 50 cm above buttresses) were mapped, tagged, and identified taxonomically (Condit, 1998).

In two additional plots, only trees  $\geq 10$  cm in dbh were included (Table S1). Trees  $< 10$  cm dbh generally contribute less than 5 % of the total AGB in mature tropical forests (Chave et al., 2003). Aboveground biomass of each individual stem was estimated using regression models based on the measured individual diameter and the wood specific gravity assigned to that species and site, or site-specific allometric equations (details in Table S1). We used only data on free-standing woody stems, and excluded

[Title Page](#)[Abstract](#)[Introduction](#)[Conclusions](#)[References](#)[Tables](#)[Figures](#)[◀](#)[▶](#)[◀](#)[▶](#)[Back](#)[Close](#)[Full Screen / Esc](#)[Printer-friendly Version](#)[Interactive Discussion](#)

lianas from our analyses. Lianas generally represent less than 5 % of the total biomass (e.g. Schnitzer et al., 2012).

The range in elevation across 19 forest plots showed a strong and significant correlation with topographic heterogeneity (Fig. S1). We therefore used the range in elevation, a metric available over all sites, as a proxy for topographic heterogeneity.

## 2.2 Sampling error in AGB

Each plot was gridded into subplots at spatial resolutions ranging from 5 to 250 m, to the extent feasible given the plot dimensions. Within each subplot, AGB ( $\text{Mg ha}^{-1}$ ) was calculated by summing AGB estimates for all trees whose stems were located within the subplot. We quantified the sampling error in AGB for subplots of area  $s$  (in ha) using the coefficient of variation of AGB among subplots, calculated as

$$\text{CV}(s) = 100 \times \frac{\sigma(s)}{\mu} \quad (1)$$

where  $\mu$  is the mean AGB in the plot,  $\sigma(s)$  is the standard deviation in AGB computed from subplots of area  $s$ , and  $\text{CV}(s)$  is the coefficient of variation for plot area  $s$  in percent. A higher CV value indicates a higher spatial heterogeneity of AGB, and therefore higher sampling error.

We focused on the CV at the 1 ha scale, denoted  $\text{CV}(1)$  in our examination of variation in sampling errors among sites. We evaluated whether  $\text{CV}(1)$  increased with AGB among sites, and whether it increased with topographic heterogeneity as quantified by the elevation range, in both cases using nonparametric Spearman rank correlations. We also tested whether  $\text{CV}(1)$  varied significantly among continents or forest types using nonparametric Kruskal–Wallis tests.

To study the spatial scaling of sampling error with plot area, we fitted power functions to the relationship between CV and subplot area. In the absence of spatial autocorrelation (i.e. given independence of each grid cell), the central limit theorem implies that  $\sigma(s) \sim \frac{1}{\sqrt{s}}$ , so the logarithm of  $\text{CV}(s)$  should decrease linearly with  $\ln(s)$ ,

BGD

11, 5711–5742, 2014

## Spatial sampling of forest biomass

M. Réjou-Méchain et al.

[Title Page](#)

[Abstract](#)

[Introduction](#)

[Conclusions](#)

[References](#)

[Tables](#)

[Figures](#)

[◀](#)

[▶](#)

[◀](#)

[▶](#)

[Back](#)

[Close](#)

[Full Screen / Esc](#)

[Printer-friendly Version](#)

[Interactive Discussion](#)



and with a slope of  $-1/2$ . Under these conditions, the sampling error of AGB is thus  $CV(s) = \frac{CV(1)}{\sqrt{s}}$ , where  $CV(1)$  is the coefficient of variation of 1 ha subplots. If spatial autocorrelation is present, we expect that  $\sigma(s) \sim \frac{1}{s^\gamma}$ , where  $\gamma \neq \frac{1}{2}$ . Positive spatial autocorrelation should yield  $\gamma < \frac{1}{2}$ ; negative spatial autocorrelation  $\gamma > \frac{1}{2}$ . To test for the significance of departure of  $\gamma$  from  $\frac{1}{2}$ , we computed 95 % confidence intervals of  $\gamma$  using  $CI = \gamma \pm t(\alpha, df) \times S_b$  where  $t$  is the Student's  $t$  distribution,  $\alpha$  the significance level (here 0.975),  $df$  the degrees of freedom (here  $n - 2$ ) and  $S_b$  the estimated standard error in the slope.

### 2.3 Spatial autocorrelation in AGB

To analyze the spatial autocorrelation of AGB within field plots, we used wavelet-kernel functions (Percival, 1995). The wavelet transform analyses the variance across spatial scales  $s$  by decomposing the signal into an orthonormal wavelet basis, in our case the isotropic Morlet wavelet (see details in Appendix S1, Supplement). A wavelet variance lower than one at a given spatial grain  $s$  indicates a negative spatial autocorrelation, i.e. neighboring subplots with an area of  $s^2$  are more different than expected under randomness, while a wavelet variance greater than one indicates positive spatial autocorrelation (neighboring subplots are more similar than expected).

At each spatial grain, we then tested whether the difference in spatial autocorrelation patterns across sites is explained by differences in topographic heterogeneity across sites using repeated and independent Spearman's rho correlation tests between the wavelet variance and the elevation range within plots.

### 2.4 Implications of field sampling error for remote sensing calibration

To assess the implications of field sampling error for remote sensing calibration, we explored the joint influence of the field plot size and of the footprint size of a hypothetical remote sensing observation on the precision of the AGB estimate. We simulated

## Spatial sampling of forest biomass

M. Réjou-Méchain et al.

[Title Page](#)

[Abstract](#)

[Introduction](#)

[Conclusions](#)

[References](#)

[Tables](#)

[Figures](#)

[◀](#)

[▶](#)

[◀](#)

[▶](#)

[Back](#)

[Close](#)

[Full Screen / Esc](#)

[Printer-friendly Version](#)

[Interactive Discussion](#)



## Spatial sampling of forest biomass

M. Réjou-Méchain et al.

[Title Page](#)

[Abstract](#)

[Introduction](#)

[Conclusions](#)

[References](#)

[Tables](#)

[Figures](#)

[◀](#)

[▶](#)

[◀](#)

[▶](#)

[Back](#)

[Close](#)

[Full Screen / Esc](#)

[Printer-friendly Version](#)

[Interactive Discussion](#)



different field-based plot sizes and also different sizes of footprints, under the best-case scenario in which the remote sensing instrument was perfectly perceptive of AGB as measured in field plots. We modeled the remote sensing footprint as circles and the calibration plots as squares to simulate the spatial mismatch between the typical

5 ground and remote sensing fields of view. We simulated field plots of 0.04, 0.1, 0.25, 0.5, 1, 2 and 4 ha centered in remote-sensing circular footprints of 0.5, 1, 2 and 4 ha (Fig. S2). We then calculated a measure of the mean error associated with the field plot – footprint comparison of AGB, ErrCV, for each combination of areas in which the field plot area is less than or equal to the footprint area as

$$10 \quad \text{ErrCV} = \frac{\sqrt{\frac{1}{N} \times \sum_{i=1}^N (\text{AGB}_{\text{footprint}, i} - \text{AGB}_{\text{subplot}, i})^2}}{\frac{1}{N} \times \sum_{i=1}^N \text{AGB}_{\text{footprint}, i} \quad (2)}$$

where  $N$  is the number of simulations (1000 per combination),  $\text{AGB}_{\text{footprint}, i}$  is the AGB measured within the remote-sensing footprint (i.e. the circle) for the  $i$ th simulation, and  $\text{AGB}_{\text{subplot}, i}$  is the AGB measured within the field subplot for that simulation. In five of our plots (Haliburton plot and the four Ituri plots), dimensions were too small to accommodate a circular 4 ha footprint and were thus not considered to calculate ErrCV at this scale.

To illustrate how field sampling error propagates into AGB maps, we then fit calibration equations from the combination of simulated remote sensing pixels and field calibration plots. For this exercise, we simulated square remote sensing pixels of 4 ha.

20 This spatial resolution mimics that of the BIOMASS mission's future instrument (Le Toan et al., 2011). Given the size of our field plots, we were able to simulate 60 such pixels (i.e. two per plot). Within each simulated pixel, we assumed that a single randomly located field plot was available for calibration, and we let the area of this field plot vary in size, from 0.01, 0.04, 0.25, 0.5, 1 and to 2 ha. We expect the calibration to 25 be of poorer quality for smaller subplots than for larger ones. To assess the goodness of fit, we calculated the regression coefficients of an ordinary least squares (OLS) lin-

ear regression between the AGB estimated in the calibration subplots of a given area and the simulated pixels. We changed the location of the subplots a thousand times and averaged the regression coefficients for each subplot size.

BGD

11, 5711–5742, 2014

It is well-established in the statistical literature that random error in the independent variable, such as that which results from sampling error in field plots, leads to systematic underestimation of the OLS regression slope, a bias referred to as attenuation or regression dilution (Fuller, 1987). This phenomenon is easily understood as the OLS slope  $\beta$  is calculated as  $\beta = \sigma^2(X, Y)/\sigma^2(X)$  where  $\sigma^2(X, Y)$  is the covariance of  $X$  and  $Y$  and  $\sigma^2(X)$  is the variance of  $X$ . If  $W$  is a measure of  $X$  with measurement error (that is,  $W = X + \varepsilon_X$ ), then  $\sigma^2(W) > \sigma^2(X)$  and  $\sigma^2(W, Y) < \sigma^2(X, Y)$  (Mcardle, 2003). Hence, the estimate of  $\beta$  tends to zero as the measurement error in  $X$  increases to infinity. In practice, this means that in the presence of error in the independent variable  $X$ , the slope of an OLS regression always is underestimated, a phenomenon referred to as the dilution bias.

Several methods have been proposed to correct for this bias (Carroll and Ruppert, 1996; Frost and Thompson, 2000; Smith, 2009). The method of moments estimator (Carroll and Ruppert, 1996; Fuller, 1987) assumes that a corrected slope,  $\beta_{MM}$ , could be calculated from the observed slope,  $\beta$ , using a reliability ratio,  $R_r$ , with

$$\beta_{MM} = \frac{\beta}{R_r} \quad (3)$$

where

$$R_r = \frac{\sigma^2(W) - \sigma^2(\varepsilon X)}{\sigma^2(W)} \quad (4)$$

To estimate  $\sigma^2(\varepsilon X)$ , the variance of the error in  $X$ , we simulated a realistic reliability study (i.e. repeated measurements in  $X$ ) and estimated  $R_r$  using the intra-class correlation coefficient (ICC), an accurate proxy for  $R_r$  (Frost and Thompson, 2000). ICC

## Spatial sampling of forest biomass

M. Réjou-Méchain et al.

[Title Page](#)

[Abstract](#)

[Introduction](#)

[Conclusions](#)

[References](#)

[Tables](#)

[Figures](#)

[◀](#)

[▶](#)

[◀](#)

[▶](#)

[Back](#)

[Close](#)

[Full Screen / Esc](#)

[Printer-friendly Version](#)

[Interactive Discussion](#)



was estimated through a one-way analysis of variance of repeated measures. We simulated “new” measurements by bootstrapping over 0.01 ha (10m × 10 m) sub-subplots for each nested subplot (i.e. 100 bootstrapped values for each of the 60 calibration plot) and calculated the ICC considering the nested subplots as factor in the one-way analysis of variance. This approach was called “within subplot  $R_r$ ”. A second reliability study approach, assuming that additional subplots (i.e. replicates) were established randomly inside the 4 ha pixel, is shown in Appendix S2 and in Fig. S3, Supplement.

We also evaluated two alternatives to OLS that have the potential to produce less bias in calibration equations. First, the Reduced Major Axis (RMA) regression minimizes the sum of squared distances both horizontally (accounting for the error in  $X$ ) and vertically (accounting for the error in  $Y$ ). Second, the nonparametric Theil–Sen estimator, also known as Sen’s slope estimator or the single median method, is the median of all the slopes determined by all pairs of sample points. Both methods have been proposed as preferred alternatives to OLS in remote sensing studies (Cohen et al., 2003; Fernandes and Leblanc, 2005; Mitchard et al., 2013a; Ryan et al., 2012).

All analyses were performed using R version 2.15.1 (R Development Core Team, 2012). The R code for the analyses is available on request from the first author.

### 3 Results

#### 3.1 Sampling error in AGB across spatial scales and forest plots

The coefficient of variation for AGB at the 1-hectare scale, CV(1), varied among sites ( $n = 30$ ) from 5.1 %, in the Haliburton plot (Canada), to 29.9 %, in the Palanan plot (Philippines), with a mean of 16.6 %, and a median of 15.2 % (Table S2). The best predictor of variation in CV(1) among plots was within-plot elevation range, that is, the difference between the highest and lowest elevation (Spearman’s rho = 0.70 and  $p < 10^{-4}$ ; Fig. 2a). Thus, topographic heterogeneity explained considerable variation in AGB heterogeneity among sites. In contrast, CV(1) was not significantly correlated

## Spatial sampling of forest biomass

M. Réjou-Méchain et al.

[Title Page](#)

[Abstract](#)

[Introduction](#)

[Conclusions](#)

[References](#)

[Tables](#)

[Figures](#)

[◀](#)

[▶](#)

[◀](#)

[▶](#)

[Back](#)

[Close](#)

[Full Screen / Esc](#)

[Printer-friendly Version](#)

[Interactive Discussion](#)



with mean AGB (Spearman's correlation test,  $p = 0.15$ ), and did not differ significantly among tropical ( $n = 20$ ), subtropical ( $n = 3$ ) and temperate ( $n = 7$ ) forests (Kruskal–Wallis test,  $p = 0.47$ ) or among continents (Kruskal–Wallis test:  $p = 0.18$ ). Asian tropical field plots tended to show higher biomass heterogeneity than other tropical field plots (median CV(1) of 24.4 and 14.3 % respectively).

Regressing the logarithm of  $CV(s)$  against  $\ln(s)$ , we found that the exponent  $\gamma$  was significantly lower than 1/2 in 15 of our 30 sites, indicating significantly positive spatial autocorrelation in AGB at about half of the sites, and significantly higher than 1/2 in only two sites, the Ituri Edoro1 plot in Democratic Republic of Congo and the Paracou plot in French Guiana (Fig. 2b, Tables S2 and S3). Sites with greater elevation range showed lower fitted  $\gamma$  values ( $\rho = -0.47$  and  $p = 0.01$ ). Such positive spatial autocorrelation means that extrapolation from 1 ha values under the assumption of no spatial autocorrelation will lead to a slight but systematic overestimation of  $CV(s)$  for areas ( $s$ ) smaller than 1 ha, and underestimation for areas larger than 1 ha (Fig. S4).

## 3.2 Spatial autocorrelation in AGB at multiple spatial scales

20 Decomposition of the variance in AGB at different spatial grains using wavelet analysis confirmed significant spatial autocorrelation of AGB in most plots (Figs. 3a, S5 and S6). There was a general trend for negative spatial autocorrelation at spatial grains of approximately 25 to 75 m and for positive spatial autocorrelation at spatial grains of 100 m and beyond (Fig. 3a). The plots with greater topographic heterogeneity were characterized by stronger spatial autocorrelation at distances > 100 m (Fig. 3b).

### 3.3 Implications of field sampling error for remote sensing calibration

We quantified how field-based sampling error scales with both field plot and remote sensing footprint areas. For very small field subplots (0.1 ha and below), sampling error was due mostly to field sampling and relatively insensitive to the footprint size (Fig. 4). For subplots and footprint size of 0.5 ha and larger, subplot area and footprint area had



## **Spatial sampling of forest biomass**

M. Réjou-Méchain et al.

Title Page

## Abstract

Introduction

## Conclusions

## References

## Tables

1

Back

**Close**

Full Screen / Esc

Interactive Discussion

similar effects on the sampling error. The error due to the spatial mismatch (circle vs. square) was much higher for small calibration plots even for a fixed ratio of the field calibration plot area to the footprint area (Fig. S8).

We explored how field-based sampling error propagate into AGB maps derived from remote sensing products. The OLS regression slope was underestimated by an average of 54 % with 0.1 ha subplots and by 37 % with 0.25 ha subplots (Fig. 5a, see examples of fits on Fig. S9). This result shows that even if though such models all correctly predict the mean AGB of the calibration plots, those with a large dilution effect (i.e. slope underestimation) would underestimate the variance in AGB, and thus systematically underestimate AGB in high AGB areas, and overestimate it in low AGB areas. Alternatives to OLS models, such as Reduced major axis (RMA) or the Theil–Sen estimator, did not fully correct for this bias (Fig. 5b). Our bias correction approach, based on bootstrapping over spatial variability within our subplots, remained too conservative, but outperformed the RMA and the Theil–Sen estimator for plots  $\geq 0.25$  ha (“within subplot  $R_r$ ” in Fig. 5b, see also Appendix S2, Supplement for another reliability study approach).

## 4 Discussion

Given the pressing need to monitor global forest carbon stocks, ecologists and remote sensing experts need to pay careful attention to accurately quantifying the errors associated with forest carbon estimates. Our results indicate that large spatial sampling error is associated with plot sizes smaller than 0.25 ha ( $> 26\%$ ). Many of the plots in standard forest inventories are much smaller than 0.25 ha and are regularly used for calibrating remote sensing models. Our findings suggest that using such small field plots to calibrate remote sensing products may lead to strong systematic biases in carbon maps.

BGD

11, 5711–5742, 2014

## Spatial sampling of forest biomass

M. Réjou-Méchain et al.

<a href="#">Title Page</a>	
<a href="#">Abstract</a>	<a href="#">Introduction</a>
<a href="#">Conclusions</a>	<a href="#">References</a>
<a href="#">Tables</a>	<a href="#">Figures</a>
<a href="#">◀</a>	<a href="#">▶</a>
<a href="#">◀</a>	<a href="#">▶</a>
<a href="#">Back</a>	<a href="#">Close</a>
<a href="#">Full Screen / Esc</a>	
<a href="#">Printer-friendly Version</a>	
<a href="#">Interactive Discussion</a>	



## 4.1 Quantifying sampling error in AGB

According to theory, sampling error in AGB decreases predictably with plot area. Previous studies have investigated the spatial scaling of sampling error in forest AGB (Baraloto et al., 2013; Chave et al., 2003; Holdaway et al., 2014; Keller et al., 2001; Wagner et al., 2010), but the present study is the first to generalize these findings across a wide range of forest types, both temperate and tropical. We found that the relative spatial sampling error in AGB averages  $\sim 16.6\%$  of the mean at 1 ha, and this error scales roughly with  $s^{-1/2}$  where  $s$  is the plot area. Sampling error tended to be larger in hilly terrain confirming that topography is a major driver of AGB heterogeneity (e.g., de Castilho et al., 2006). This result suggests that forest biomass maps in hilly areas have larger uncertainties, and that sampling designs should take topography into account. This is an important finding given that 23 % of the world's forests are on hilly terrain (Table S4). We found no other systematic trends among continents or forest types or with mean AGB. Asian tropical forests displayed higher sampling errors than other tropical sites, but this could be explained by the larger topographic heterogeneity in our tropical Asian study sites (Table S1). This finding is no accident of our study locations; remaining old-growth tropical forests in Asia are disproportionately located in topographically complex terrain, more so than on other continents (Table S4), probably because these areas have disproportionately escaped human disturbance.

The careful quantification of spatial sampling error described here should be useful in providing guidelines for forest inventory design at the national scale, as well as in remote sensing applications (see below). It should, however, be borne in mind that we focused on errors resulting from spatial sampling and ignored other sources of error which also contribute significantly to uncertainty in AGB estimates, including errors in field measurements (e.g. diameter and height measurements or wood density attribution through floristic identification; Flores and Coomes, 2011; Larjavaara and Muller-Landau, 2013), data cleaning procedures (Muller-Landau et al., 2014), biomass allometries (Chave et al., 2004; Molto et al., 2013), and wood carbon content (Thomas

## Spatial sampling of forest biomass

M. Réjou-Méchain et al.

[Title Page](#)

[Abstract](#)

[Introduction](#)

[Conclusions](#)

[References](#)

[Tables](#)

[Figures](#)

◀

▶

◀

▶

[Back](#)

[Close](#)

[Full Screen / Esc](#)

[Printer-friendly Version](#)

[Interactive Discussion](#)



and Martin, 2012). Finally, we focused on AGB stocks; sampling error in AGB changes is far larger due to the low frequency of AGB loss events (Chambers et al., 2013; Muller-Landau et al., 2014; Wagner et al., 2010).

## 4.2 Spatial autocorrelation in AGB and consequences for field sampling

- 5 The wavelet analysis revealed that most study sites displayed significant spatial autocorrelation in AGB with contrasting patterns at different spatial grains. On average, a negative autocorrelation occurred at spatial grains between 25 and 75 m. Hence, neighboring field plots ranging in size from 25 m × 25 m to 75 m × 75 m tend to provide less similar AGB estimates than plots that are separated by greater distances. Such  
10 negative autocorrelation pattern may be interpreted as the effect of spatially localized AGB changes due to treefall gap openings. For instance, in a Neotropical forest of French Guiana, van der Meer and Bongers (1996) found that the effects of large tree gaps typically occur at such spatial grains. As AGB is mainly shaped by large trees, another explanation may lie in the nature of the spatial distribution of these large trees  
15 (Lutz et al., 2013). Both competition for below- and aboveground resources among individuals and Janzen–Connell-type effects in large diameter species may generate strong density-dependence between large trees, and thus negative autocorrelation pattern in AGB. At larger distances ( $\geq 100$  m), AGB was positively autocorrelated in many sites, and significantly so, with the degree of autocorrelation positively related to topographical heterogeneity, a feature known to influence forest structure (e.g. de Castilho et al., 2006; McEwan et al., 2011). Thus, 1 ha and larger plots are expected to be statistically more representative of a larger remote sensing footprint area than expected  
20 under the null hypothesis of no spatial correlation.

The spatial structures we found have implications for optimal plot sampling designs for forest inventories. Negative or nonexistent spatial autocorrelation at scales less than 100 m suggests that there is generally no gain in representativeness from locating multiple small plots within a small area or footprint ( $\leq 100$  m) rather than establishing one or few larger plots in the same area. That is, because neighboring small plots are just



as different, if not more different, from a focal plot than more distantly located small plots. Therefore expanding a single small plot provides similar or more information than adding another small plot nearby. A number of forest inventory designs use clusters of very small plots ( $\leq 0.04$  ha); e.g., the US Forest Service Forest Inventory and

- 5 Analysis program (Bechtold and Patterson, 2005). These cluster designs have distinct disadvantages for calibrating remote sensing products as their small dimensions are below the resolution of most sensors (see below), and their edge to area ratios are higher than single larger plots of the same total area. Although small plots may have practical advantages in field sampling, these should be carefully weighed against the  
10 above-mentioned disadvantages.

In contrast, significant spatial autocorrelation of AGB at scales larger than 100 m suggests that many intermediate scale plots of  $\sim 0.25\text{--}1$  ha will better approximate the mean AGB of a landscape than fewer large plots having the same total surveyed area. This would be especially true if such a sampling design was stratified according to  
15 topography. However, as discussed below, small plots may lead to strong systematic biases and errors when used individually for calibrating remote sensing products of larger resolution.

### 4.3 Field sampling error and remote sensing of carbon stocks

As expected, sampling error depends both on field plot area and on the size of the  
20 remote sensing footprint. However, when field subplots were very small (0.1 ha and below), the uncertainty was due mostly to field sampling, and was relatively insensitive to the footprint area. For subplots and footprints of 0.5–4.0 ha, both subplot and footprint areas have strong effects on sampling error. We also found that error was much lower for large calibration plots even when the same ratio of calibration plot area to  
25 footprint area was maintained. This reflects decreasing edge-to-area ratios for larger area, which also provide other advantages to larger plots (Mascaro et al., 2011; see also Zolkos et al., 2013).

<a href="#">Title Page</a>	
<a href="#">Abstract</a>	<a href="#">Introduction</a>
<a href="#">Conclusions</a>	<a href="#">References</a>
<a href="#">Tables</a>	<a href="#">Figures</a>
<a href="#">◀</a>	<a href="#">▶</a>
<a href="#">◀</a>	<a href="#">▶</a>
<a href="#">Back</a>	<a href="#">Close</a>
<a href="#">Full Screen / Esc</a>	
<a href="#">Printer-friendly Version</a>	
<a href="#">Interactive Discussion</a>	



Our analyses show that field-sampling strategy may result in a serious bias in model calibration of remote sensing products. When this bias is present, inversion models return AGB values that are regressed to the mean of the calibration plots (Fig. 5a), and thus underestimate the true spatial AGB variance. For instance, in a recent study

5 that used 112 circular 0.13 ha plots to calibrate L-band radar products (Carreiras et al., 2012), the slope of an OLS regression was found to be underestimated by 86 % and the final AGB map displayed a much lower variance than the global map produced by Saatchi et al. (2011). The dilution bias is independent of the number of calibration plots, and it depends only on the size (and thus sampling error) of these plots. In addition such  
10 an inversion model estimates is expected to estimate the mean AGB of the sampling plots correctly (Fig. 5a), but the mean of a biomass map may still seriously be biased, unless calibration plots are truly representative of the AGB for the mapped area.

We tested several alternative approaches to OLS regression and found that the best way to diminish this bias is to bootstrap over spatial variability within subplots and to  
15 correct the estimated slope using these simulated “replicates”. Some remote sensing studies have argued that alternative to OLS regression such as RMA or the Theil–Sen estimator are good alternatives to OLS regression when errors occur in  $X$  (Cohen et al., 2003; Fernandes and Leblanc, 2005; Mitchard et al., 2013a; Ryan et al., 2012). Here, we showed that these alternatives do not resolve the dilution bias and still provide  
20 strongly biased products. Furthermore, the use of RMA is contentious (Carroll and Ruppert, 1996; Smith, 2009), especially if the primary purpose of the regression equation is prediction (Legendre and Legendre, 1998). Sampling error propagation in other empirical calibration approaches should be carefully explored in the future.

The best way to avoid the dilution bias is to use calibration plots covering entire  
25 remote sensing pixels. For remote sensing tools with a resolution on the order of 4 ha, such as the planned BIOMASS mission, it is realistic to invest in a network of similarly-sized field calibration plots. Though such field sampling is expensive, it would greatly improve the basis for mapping forest biomass. An alternative is to calibrate coarse-resolution remote sensing with higher-resolution remote sensing such as airborne Li-

## Spatial sampling of forest biomass

M. Réjou-Méchain et al.

[Title Page](#)[Abstract](#)[Introduction](#)[Conclusions](#)[References](#)[Tables](#)[Figures](#)[◀](#)[▶](#)[◀](#)[▶](#)[Back](#)[Close](#)[Full Screen / Esc](#)[Printer-friendly Version](#)[Interactive Discussion](#)

DAR, which is itself well calibrated with smaller plots (Mascaro et al., 2011). In these cases, care must be taken that errors and uncertainties are carefully and appropriately propagated through the two-stage calibration to the final map (Asner et al., 2013).

## 5 Conclusion

- 5 Accurate measurements of forest carbon stocks are critical to reduce uncertainties in the global carbon budget. However, uncertainty associated with forest carbon map products, from either field based and/or remote-sensing approaches, has been overlooked in most studies. In this paper, we used a large-scale global dataset to illustrate that high spatial variability in AGB within forested sites leads to large sampling error at
- 10 standard plot sizes (< 0.25 ha). Topographical heterogeneity is a major source of sampling error and should be thus explicitly accounted for in future sampling scheme. We also show that remote sensing products that rely on field data for calibration may be highly biased if field-sampling error is large. Such biases have previously been ignored by the remote sensing community and, as we show, can only be partially corrected by
- 15 statistical methods alone. Overall, our results strongly suggest that more large forest plots (> 0.25 ha) are needed to enable accurate calibration of remote sensing estimates of forest carbon. We hope that this contribution will stimulate further work on field sampling error propagation to remote sensing products and that future studies will pay more careful attention to field sampling strategies.

- 20 **Supplementary material related to this article is available online at  
[http://www.biogeosciences-discuss.net/11/5711/2014/  
bgd-11-5711-2014-supplement.pdf](http://www.biogeosciences-discuss.net/11/5711/2014/bgd-11-5711-2014-supplement.pdf).**

*Acknowledgements.* We are grateful to all the people, institutions, foundations, and funding bodies that have contributed to the collection of the large plot datasets (<http://www.ctfs.si.edu/>



group/Partners/Collaborating+Institutions for the CTFS plots), including the staff members and central office of the Amacayacu National Natural Park of Colombia. We sincerely thank Erika Gonzalez and Sandeep Pulla for their help with analyses for the SCBI and Mudumalai plots, respectively. Financial support for the analyses presented here was provided by the CNES (postdoctoral grant to MRM), the National Science Foundation (DEB #1046113), and two “Investissement d’Avenir” grants managed by Agence Nationale de la Recherche (CEBA: ANR-10-LABX-25-01; TULIP: ANR-10-LABX-0041).

## References

- Abdalati, W., Zwally, H. J., Bindschadler, R., Csatho, B., Farrell, S. L., Fricker, H. A., Harding, D.,  
10 Kwok, R., Lefsky, M., Markus, T., Marshak, A., Neumann, T., Palm, S., Schutz, B., Smith, B.,  
Spinhirne, J., and Webb, C.: The ICESat-2 Laser Altimetry Mission, *Proceedings of the IEEE*,  
98, 735–751, doi:10.1109/JPROC.2009.2034765, 2010.
- Asner, G. P., Powell, G. V. N., Mascaro, J., Knapp, D. E., Clark, J. K., Jacobson, J.,  
15 Kennedy-Bowdoin, T., Balaji, A., Paez-Acosta, G., Victoria, E., Secada, L., Valqui, M., and  
Hughes, R. F.: High-resolution forest carbon stocks and emissions in the Amazon, *P. Natl.  
Acad. Sci. USA*, 107, 16738–16742, doi:10.1073/pnas.1004875107, 2010.
- Asner, G. P., Mascaro, J., Anderson, C., Knapp, D. E., Martin, R. E., Kennedy-Bowdoin, T.,  
15 Breugel, M. van, Davies, S., Hall, J. S., Muller-Landau, H. C., Potvin, C., Sousa, W., Wright, J.,  
and Bermingham, E.: High-fidelity national carbon mapping for resource management and  
REDD+, *Carbon Balance and Management*, 8, 1–14, doi:10.1186/1750-0680-8-7, 2013.
- Baccini, A., Friedl, M. A., Woodcock, C. E., and Zhu, Z.: Scaling field data to calibrate and  
20 validate moderate spatial resolution remote sensing models, *Photogramm. Eng. Rem. S.*,  
73, 945–954, 2007.
- Baccini, A., Goetz, S. J., Walker, W. S., Laporte, N. T., Sun, M., Sulla-Menashe, D., Hackler, J.,  
25 Beck, P. S. A., Dubayah, R., Friedl, M. A., Samanta, S., and Houghton, R. A.: Estimated car-  
bon dioxide emissions from tropical deforestation improved by carbon-density maps, *Nature  
Climate Change*, 2, 182–185, doi:10.1038/nclimate1354, 2012.
- Baraloto, C., Molto, Q., Rabaud, S., Hérault, B., Valencia, R., Blanc, L., Fine, P. V. A., and  
Thompson, J.: Rapid simultaneous estimation of aboveground biomass and tree diversity

across neotropical forests: a comparison of field inventory methods, *Biotropica*, 45, 288–298, doi:10.1111/btp.12006, 2013.

Bechtold, W. A. and Patterson, P. L.: The Enhanced Forest Inventory and Analysis Program: National Sampling Design and Estimation Procedures, US Department of Agriculture Forest Service, Southern Research Station, available at: [http://www.srs.fs.usda.gov/pubs/gtr/gtr\\_srs080/gtr\\_srs080](http://www.srs.fs.usda.gov/pubs/gtr/gtr_srs080/gtr_srs080) (last access: 18 September 2013), 2005.

Bontemps, S., Defourny, P., Van Bogaert, E., Arino, O., Kalogirou, V., and Ramos Perez, J.: GLOBCOVER 2009 Products Description and Validation Report, available at: [https://globcover.s3.amazonaws.com/LandCover2009/GLOBCOVER2009\\_Validation\\_Report\\_1.0.pdf](https://globcover.s3.amazonaws.com/LandCover2009/GLOBCOVER2009_Validation_Report_1.0.pdf), 2011.

Carreiras, J. M. B., Vasconcelos, M. J., and Lucas, R. M.: Understanding the relationship between aboveground biomass and ALOS PALSAR data in the forests of Guinea-Bissau (West Africa), *Remote Sens. Environ.*, 121, 426–442, doi:10.1016/j.rse.2012.02.012, 2012.

Carroll, R. J. and Ruppert, D.: The use and misuse of orthogonal regression in linear errors-in-variables models, *Am. Stat.*, 50, 1–6, doi:10.1080/00031305.1996.10473533, 1996.

Chambers, J. Q., Negron-Juarez, R. I., Marra, D. M., Vittorio, A. D., Tews, J., Roberts, D., Ribeiro, G. H. P. M., Trumbore, S. E., and Higuchi, N.: The steady-state mosaic of disturbance and succession across an old-growth Central Amazon forest landscape, *P. Natl. Acad. Sci. USA*, 110, 3949–3954, doi:10.1073/pnas.1202894110, 2013.

Chave, J., Condit, R., Lao, S., Caspersen, J. P., Foster, R. B., and Hubbell, S. P.: Spatial and temporal variation of biomass in a tropical forest: results from a large census plot in Panama, *J. Ecol.*, 91, 240–252, 2003.

Chave, J., Condit, R., Aguilar, S., Hernandez, A., Lao, S., and Perez, R.: Error propagation and scaling for tropical forest biomass estimates, *Philos. T. R. Soc. B*, 359, 409–420, 2004.

Chave, J., Condit, R., Muller-Landau, H. C., Thomas, S. C., Ashton, P. S., Bunyavejchewin, S., Co, L. L., Dattaraja, H. S., Davies, S. J., Esufali, S., Ewango, C. E. N., Feeley, K. J., Foster, R. B., Gunatilleke, N., Gunatilleke, S., Hall, P., Hart, T. B., Hernández, C., Hubbell, S. P., Itoh, A., Kiratiprayoon, S., LaFrankie, J. V., Loo de Lao, S., Makana, J.-R., Noor, M. N. S., Kasim, A. R., Samper, C., Sukumar, R., Suresh, H. S., Tan, S., Thompson, J., Tongco, M. D. C., Valencia, R., Vallejo, M., Villa, G., Yamakura, T., Zimmerman, J. K., and Losos, E. C.: Assessing evidence for a pervasive alteration in tropical tree communities, *PLoS Biol.*, 6, 3e45 doi:10.1371/journal.pbio.0060045, 2008.

Spatial sampling of forest biomass

M. Réjou-Méchain et al.

Title Page

Abstract

Introduction

Conclusions

References

Tables

Figures

◀

▶

◀

▶

Back

Close

Full Screen / Esc

Printer-friendly Version

Interactive Discussion



## Spatial sampling of forest biomass

M. Réjou-Méchain et al.

[Title Page](#)

[Abstract](#)

[Introduction](#)

[Conclusions](#)

[References](#)

[Tables](#)

[Figures](#)

[◀](#)

[▶](#)

[◀](#)

[▶](#)

[Back](#)

[Close](#)

[Full Screen / Esc](#)

[Printer-friendly Version](#)

[Interactive Discussion](#)



**Spatial sampling of forest biomass**

M. Réjou-Méchain et al.

Keller, M., Palace, M., and Hurt, G.: Biomass estimation in the Tapajos National Forest, Brazil: examination of sampling and allometric uncertainties, *Forest Ecol. Manag.*, 154, 371–382, doi:10.1016/S0378-1127(01)00509-6, 2001.

Larjavaara, M. and Muller-Landau, H. C.: Measuring tree height: a quantitative comparison of two common field methods in a moist tropical forest, *Methods in Ecology and Evolution*, 4, 793–801, doi:10.1111/2041-210X.12071, 2013.

Le Toan, T., Quegan, S., Davidson, M. W. J., Balzter, H., Paillou, P., Papathanassiou, K., Plummer, S., Rocca, F., Saatchi, S., Shugart, H., and Ulander, L.: The BIOMASS mission: mapping global forest biomass to better understand the terrestrial carbon cycle, *Remote Sens. Environ.*, 115, 2850–2860, doi:10.1016/j.rse.2011.03.020, 2011.

Legendre, P. and Legendre, L.: *Numerical Ecology*, 2nd edn., Elsevier Science BV, Amsterdam, 1998.

Lewis, S. L., Lopez-Gonzalez, G., Sonké, B., Affum-Baffoe, K., Baker, T. R., Ojo, L. O., Phillips, O. L., Reitsma, J. M., White, L., Comiskey, J. A., K, M.-N. D., Ewango, C. E. N., Feldpausch, T. R., Hamilton, A. C., Gloor, M., Hart, T., Hladik, A., Lloyd, J., Lovett, J. C., Makana, J.-R., Malhi, Y., Mbago, F. M., Ndangalasi, H. J., Peacock, J., Peh, K. S.-H., Sheil, D., Sunderland, T., Swaine, M. D., Taplin, J., Taylor, D., Thomas, S. C., Votere, R., and Wöll, H.: Increasing carbon storage in intact African tropical forests, *Nature*, 457, 1003–1006, doi:10.1038/nature07771, 2009.

Losos, E. C. and Leigh, E. G.: The growth of a tree plot network, in: *Tropical Forest Diversity and Dynamism: Findings from a Large-Scale Plot Network*, 3–7, 2004.

Lutz, J. A., Larson, A. J., Freund, J. A., Swanson, M. E., and Bible, K. J.: The importance of large-diameter trees to forest structural heterogeneity, *PLOS ONE*, 8, e82784, doi:10.1371/journal.pone.0082784, 2013.

Malhi, Y., Wood, D., Baker, T. R., Wright, J., Phillips, O. L., Cochrane, T., Meir, P., Chave, J., Almeida, S., Arroyo, L., Higuchi, N., Killeen, T. J., Laurance, S. G., Laurance, W. F., Lewis, S. L., Monteagudo, A., Neill, D. A., Vargas, P. N., Pitman, N. C. A., Quesada, C. A., Salomão, R., Silva, J. N. M., Lezama, A. T., Terborgh, J., Martínez, R. V., and Vinceti, B.: The regional variation of aboveground live biomass in old-growth Amazonian forests, *Glob. Change Biol.*, 12, 1107–1138, doi:10.1111/j.1365-2486.2006.01120.x, 2006.

Mascaro, J., Detto, M., Asner, G. P., and Muller-Landau, H. C.: Evaluating uncertainty in mapping forest carbon with airborne LiDAR, *Remote Sens. Environ.*, 115, 3770–3774, doi:10.1016/j.rse.2011.07.019, 2011.

[Title Page](#)[Abstract](#)[Introduction](#)[Conclusions](#)[References](#)[Tables](#)[Figures](#)[◀](#)[▶](#)[◀](#)[▶](#)[Back](#)[Close](#)[Full Screen / Esc](#)[Printer-friendly Version](#)[Interactive Discussion](#)

**Spatial sampling of forest biomass**

M. Réjou-Méchain et al.

- McArdle, B. H.: Lines, models, and errors: regression in the field, *Limnol. Oceanogr.*, 48, 1363–1366, 2003.
- McEwan, R. W., Lin, Y.-C., Sun, I.-F., Hsieh, C.-F., Su, S.-H., Chang, L.-W., Song, G.-Z. M., Wang, H.-H., Hwong, J.-L., Lin, K.-C., Yang, K.-C., and Chiang, J.-M.: Topographic and biotic regulation of aboveground carbon storage in subtropical broad-leaved forests of Taiwan, *Forest Ecol. Manag.*, 262, 1817–1825, doi:10.1016/j.foreco.2011.07.028, 2011.
- Mermoz, S., Le Toan, T., Villard, L., Réjou-Méchain, M., and Seifert-Granzin, J.: Biomass assessment in the Cameroon savanna using ALOS PALSAR data, *Remote Sens. Environ.*, in press, 2014.
- Miles, L. and Kapos, V.: Reducing greenhouse gas emissions from deforestation and forest degradation: global land-use implications, *Science*, 320, 1454–1455, doi:10.1126/science.1155358, 2008.
- Mitchard, E. T. A., Meir, P., Ryan, C. M., Woollen, E. S., Williams, M., Goodman, L. E., Mucavele, J. A., Watts, P., Woodhouse, I. H., and Saatchi, S. S.: A novel application of satellite radar data: measuring carbon sequestration and detecting degradation in a community forestry project in Mozambique, *Plant Ecology & Diversity*, 6, 159–170, doi:10.1080/17550874.2012.695814, 2013a.
- Mitchard, E. T. A., Saatchi, S. S., Baccini, A., Asner, G. P., Goetz, S. J., Harris, N., and Brown, S.: Uncertainty in the spatial distribution of tropical forest biomass: a comparison of pan-tropical maps, *Carb Bal Manage*, available at: <http://www.biomedcentral.com/content/pdf/1750-0680-8-10.pdf> (last access: 28 January 2014), 2013b.
- Molto, Q., Rossi, V., and Blanc, L.: Error propagation in biomass estimation in tropical forests, *Methods in Ecology and Evolution*, 4, 175–183, doi:10.1111/j.2041-210x.2012.00266.x, 2013.
- Muller-Landau, H. C., Detto, M., Chisholm, R. A., Hubbel, S. P., and Condit, R.: Detecting and projecting changes in forest biomass from plot data, in: *Forests and Global Change*, edited by: Coomes, D. A. and Burslem, D., available at: [http://books.google.fr/books?hl=fr&lr=&id=QHdYAgAAQBAJ&oi=fnd&pg=PA381&dq=detecting+and+projecting+changes+biomass+condit+detto&ots=HSziWpN2aa&sig=nufRDPI5gMMHYibmapP2b\\_4-4Yc](http://books.google.fr/books?hl=fr&lr=&id=QHdYAgAAQBAJ&oi=fnd&pg=PA381&dq=detecting+and+projecting+changes+biomass+condit+detto&ots=HSziWpN2aa&sig=nufRDPI5gMMHYibmapP2b_4-4Yc) (last access: 22 December 2013), 381–415, 2014.
- Pan, Y., Birdsey, R. A., Fang, J., Houghton, R., Kauppi, P. E., Kurz, W. A., Phillips, O. L., Shvidenko, A., Lewis, S. L., and Canadell, J. G.: A large and persistent carbon sink in the world's forests, *Science*, 333, 988–993, 2011.

[Title Page](#)[Abstract](#)[Introduction](#)[Conclusions](#)[References](#)[Tables](#)[Figures](#)[◀](#)[▶](#)[◀](#)[▶](#)[Back](#)[Close](#)[Full Screen / Esc](#)[Printer-friendly Version](#)[Interactive Discussion](#)

**Spatial sampling of forest biomass**

M. Réjou-Méchain et al.

[Title Page](#)[Abstract](#)[Introduction](#)[Conclusions](#)[References](#)[Tables](#)[Figures](#)[◀](#)[▶](#)[◀](#)[▶](#)[Back](#)[Close](#)[Full Screen / Esc](#)[Printer-friendly Version](#)[Interactive Discussion](#)

- Thomas, S. C. and Martin, A. R.: Carbon content of tree tissues: a synthesis, *Forests*, 3, 332–352, doi:10.3390/f3020332, 2012.
- Van der Meer, P. J. and Bongers, F.: Patterns of tree-fall and branch-fall in a tropical rain forest in french guiana, *J. Ecol.*, 84, 19–29, doi:10.2307/2261696, 1996.
- Wagner, F., Rutishauser, E., Blanc, L., and Herault, B.: Effects of plot size and census interval on descriptors of forest structure and dynamics, *Biotropica*, 42, 664–671, doi:10.1111/j.1744-7429.2010.00644.x, 2010.
- Wulder, M. A., White, J. C., Nelson, R. F., Næsset, E., Ørka, H. O., Coops, N. C., Hilker, T., Bater, C. W., and Gobakken, T.: Lidar sampling for large-area forest characterization: a review, *Remote Sens. Environ.*, 121, 196–209, doi:10.1016/j.rse.2012.02.001, 2012.
- Zolkos, S. G., Goetz, S. J., and Dubayah, R.: A meta-analysis of terrestrial aboveground biomass estimation using lidar remote sensing, *Remote Sens. Environ.*, 128, 289–298, doi:10.1016/j.rse.2012.10.017, 2013.

[Title Page](#)

[Abstract](#)

[Introduction](#)

[Conclusions](#)

[References](#)

[Tables](#)

[Figures](#)

◀

▶

◀

▶

[Back](#)

[Close](#)

[Full Screen / Esc](#)

[Printer-friendly Version](#)

[Interactive Discussion](#)



**Spatial sampling of forest biomass**

M. Réjou-Méchain et al.

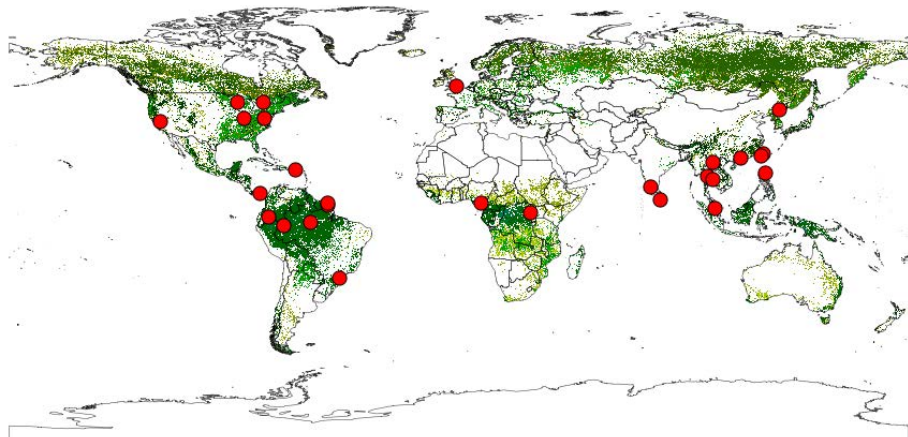


**Fig. 1.** Study sites. Geographical distribution of the 30 sites (red points) included in the present study. Note that the four sites at Ituri (Democratic Republic of Congo) are represented by a single dot due to their proximity. Forest distribution is shown in green (from Bontemps et al., 2011). Details on study sites are provided in Table S1.

[Title Page](#)[Abstract](#)[Introduction](#)[Conclusions](#)[References](#)[Tables](#)[Figures](#)[◀](#)[▶](#)[◀](#)[▶](#)[Back](#)[Close](#)[Full Screen / Esc](#)[Printer-friendly Version](#)[Interactive Discussion](#)

## Spatial sampling of forest biomass

M. Réjou-Méchain et al.

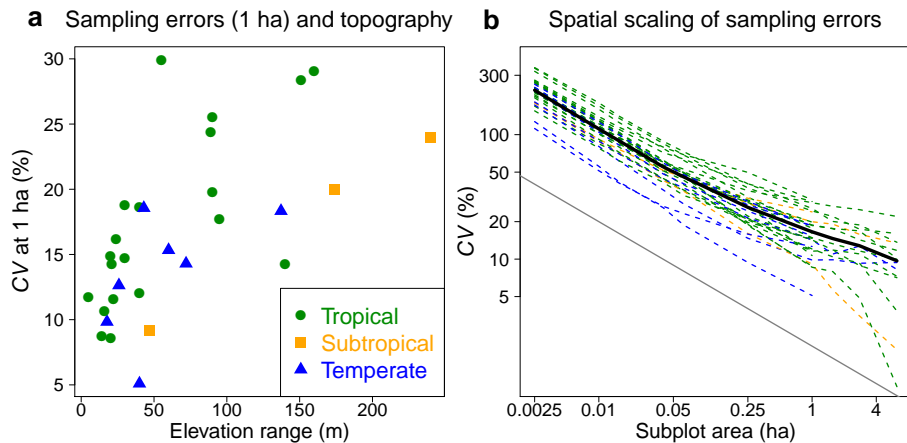


**Fig. 2.** Sampling error as a function of topographic heterogeneity and of spatial scale. **(a)** represents the coefficient of variation for AGB at the 1 hectare scale,  $CV(1)$ , as a function of elevation range (the difference between highest and lowest altitude in the plot) for each of the plots. **(b)** shows the spatial scaling of sampling error in AGB within sites, from 0.0025 ha to 6.25 ha. The coefficients of variation ( $CV(s)$ ) of AGB for individual sites (dotted lines) and means over all sites (solid black line) as a function of subplot area, are compared with the theoretical slope of  $-0.5$  (on these log–log axes), in the absence of spatial autocorrelation in AGB (solid grey line). Separate graphs for each individual site are provided in Fig. S4 and separate graphs according to the topographic heterogeneity are provided in Fig. S5.

- [Title Page](#)
- [Abstract](#) [Introduction](#)
- [Conclusions](#) [References](#)
- [Tables](#) [Figures](#)
- [◀](#) [▶](#)
- [◀](#) [▶](#)
- [Back](#) [Close](#)
- [Full Screen / Esc](#)
- [Printer-friendly Version](#)
- [Interactive Discussion](#)

## Spatial sampling of forest biomass

M. Réjou-Méchain et al.

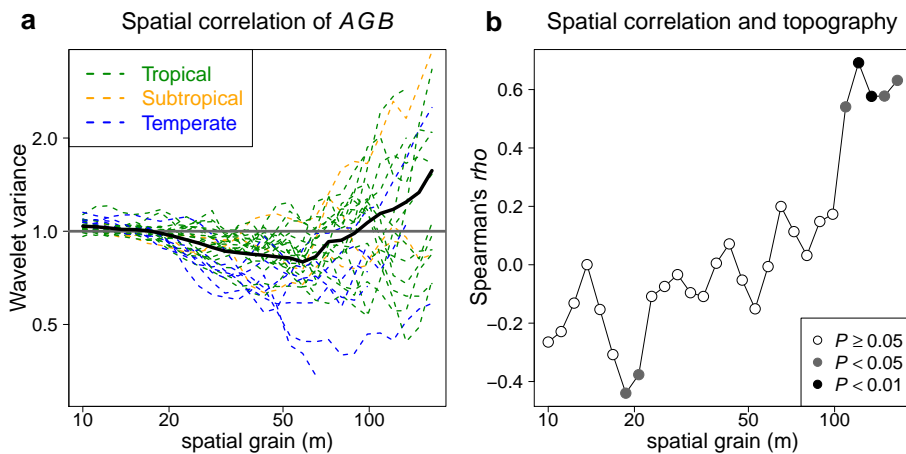


**Fig. 3.** Scale-dependent patterns of spatial autocorrelation in AGB and relationship to topographic heterogeneity. **(a)** shows the spatial grain-dependent patterns of spatial autocorrelation in AGB as reflected in the wavelet variance as a function of spatial grain for each site (dashed lines), together with the ensemble average across all sites (solid black line). In the absence of spatial autocorrelation the wavelet variance is expected to equal one irrespective of spatial grain (solid grey line). A wavelet variance lower than one at a given spatial grain (e.g., the average for 25–75 m) indicates overdispersion at that spatial grain, while a wavelet variance greater than one (e.g., the average for > 100 m) indicates clustering at that spatial grain. **(b)** shows the Spearman's  $\rho$  correlation of the elevation range with the wavelet variance among sites, as a function of spatial grain at which the wavelet variance is computed.  $P$  values of the Spearman's  $\rho$  correlation tests are provided within the panel and indicate that significant negative correlations between the wavelet variance and the topographic relief occur at spatial grains of approximately 20 m, while strong and significant positive correlations occur at spatial grains above 100 m. Separate graphs for each site, with confidence intervals for the null hypothesis of no spatial correlation, are shown in Fig. S6; separate graphs with sites grouped by topographic heterogeneity are shown in Fig. S7.

**Spatial sampling of forest biomass**

M. Réjou-Méchain et al.

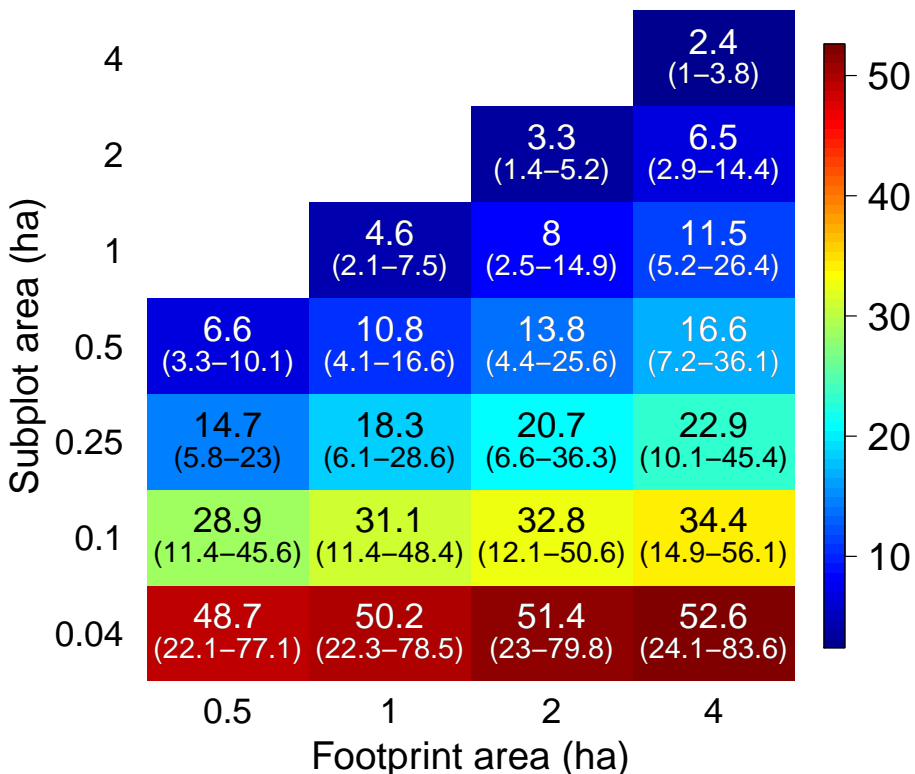


**Fig. 4.** Expected errors when the calibration/validation plots and the remote sensing footprint differ in shape and size. The remote sensing footprint is assumed circular, and subplots are assumed to be square to simulate the spatial mismatch between the remote sensing signal and the calibration plot. The mean ErrCV in AGB estimates across all sites ( $n = 30$ ) is given within the figure and the range of ErrCV across sites is given in parentheses below the mean.

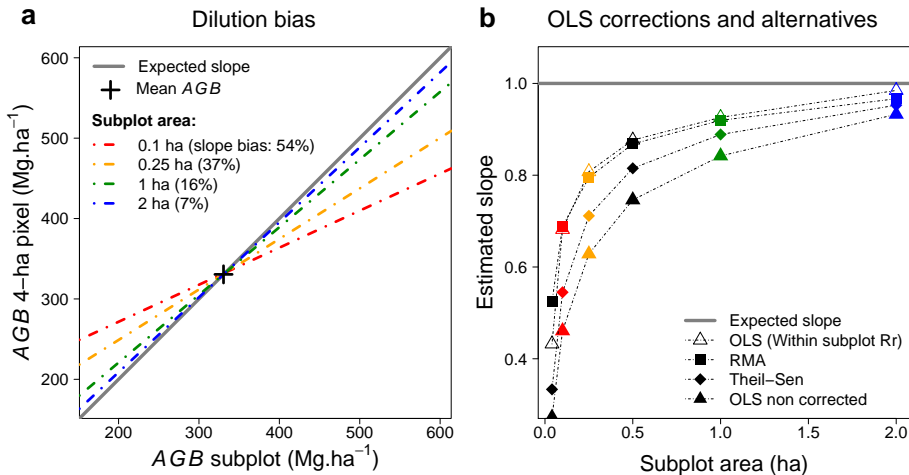


**Fig. 5.** Propagation of field sampling error to remote sensing products: the dilution bias. **(a)** illustrates the mean regression lines obtained from an OLS linear regression between the AGB estimated within 4 ha pixels randomly established in large plots ( $n = 60$ , dependent variable) and variable-size subplots located within these pixels (independent variable). Different subplot areas were simulated (see key). An unbiased estimated slope should be equal to one. Slope dilution biases associated with each subplot area are provided in parentheses. All the lines cross at the mean AGB over all sites showing that the regression correctly predicts the mean AGB of the calibration plots. However, the smaller the subplot, the more regressed to the mean the predictions. **(b)** shows how the estimated slope varies under different potential correction methods (see key) and with subplot area, compared with the true slope of one (solid grey line).

- [Title Page](#)
- [Abstract](#) [Introduction](#)
- [Conclusions](#) [References](#)
- [Tables](#) [Figures](#)
- [◀](#) [▶](#)
- [◀](#) [▶](#)
- [Back](#) [Close](#)
- [Full Screen / Esc](#)
- [Printer-friendly Version](#)
- [Interactive Discussion](#)